This paper describes objective technical results and analysis. Any subjective views or opinions that might be expressed in the paper do not necessarily represent the views of the U.S. Department of Energy or the United States Government.

SAND2022-14488C

Indium Interconnect Mechanical Performance with Variable UBM and Decreasing Bump Size

Rebecca Wheeling, Ph.D.
Sandia National Laboratories
NM, USA
rwheeli@sandia.gov

Jeier Yang, Matt Jordan, N. Scott Bobbitt, Ben White, Mieko Hirabayashi
Sandia National Laboratories
NM, USA

"Sandia National Laboratories is a multimission laboratory managed and operated by National Technology & Engineering Solutions of Sandia, LLC, a wholly owned subsidiary of Honeywell International Inc., for the U.S. Department of Energy's National Nuclear Security Administration under contract DE-NA0003525."

ABSTRACT

Indium is used to integrate disparate semiconductor materials because of its ability to cold weld and its high ductility, even at cryogenic temperatures. Previous work used a cryogenic focus ion beam (cryo-FIB) and scanning electron microscopy (SEM) to quantify the kinetics if intermetallic growth for 3 separate underbump metallurgies (UBMs) found in literature: Thin Ti/Ni, thin Ti/Ni/Au, and thick Ti/Ni.

Current work seeks to better understand how the indium (In) bump size affects the respective interface kinetics and subsequent mechanical properties. Indium bumps ranging from 4-14 um were aged 1 day at 125 °C (guided by the previous results). Interfacial evolution was characterized and compared using the cryo-FIB technique. Effect on mechanical performance was evaluated by shearing as-fabricated and aged bumps. Atomistic modeling of the interface reactions, relying on density functional theory and molecular dynamics, will complement the metallurgical and mechanical analyses.

Pure indium was selected for this study because it is a commonly used single element interconnect in electronic applications that readily reacts, so it serves as a simpler case for modeling. The basis of this study will be used for board-level SnPb and Pb-free solder interconnects, where continuum modeling dominates current lifetime predictions. The eventual objective is to determine if/when interconnect sizes approach a size scale that requires atomistic considerations to maintain accurate solder behavior predictions.

Keywords: Indium micro bumps, Interfaces, Aging, Reliability

INTRODUCTION

Indium microbumps are attractive for a variety of reasons: they can integrate disparate semiconductor materials, their high ductility supports cold welding/bonding which prevents stresses from flip chip operations and accommodates strain and CTE mismatches, even at cryogenic temperatures [1].

For these reasons, indium bump bonding is a common method for integrating focal plane arrays for a cryogenic spectrometers [2] Josephson junctions for quantum computing [3], and HgCdTe IR detectors [4,5]. There may also be benefits to a flip chip bonding approach utilizing indium for InGaP/InGaAs/Si multijunction solar power [6-8].

As shown in Figure 1, use conditions for In bump bond interconnects are generally integrated within the device level, rather than at a board level. So, heterogeneous integration concepts, which seek to incorporate multiple components/devices into one larger component/device, in more of a modular sense depend on the performance and reliability of these kinds of interconnection strategies.
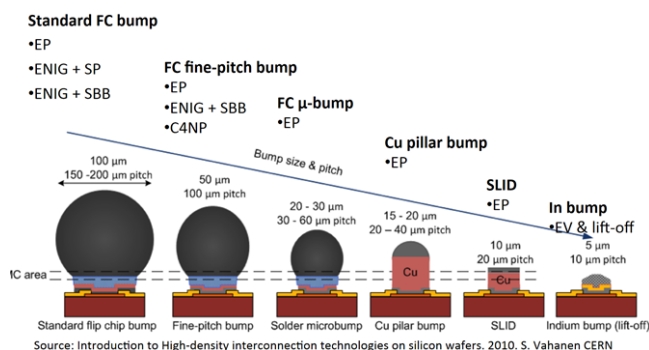

Figure 1.Schematic showing various sized bump interconnects, from larger to smaller, left to right [9].

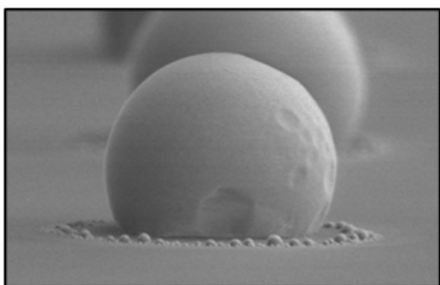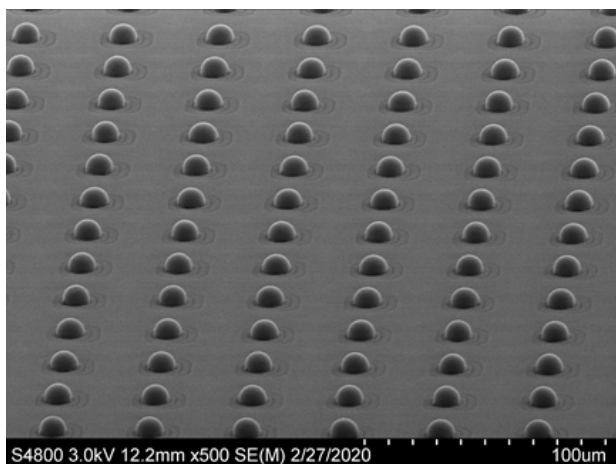The SEM image in Figure 2 shows an indium bump array fabricated at Sandia.

Figure 2. SEM image of an array of In bumps, fabricated at Sandia, courtesy of Matt Jordan.

Despite its wide and diverse use, understanding the reliability of indium microbumps is limited by the complex metallurgy occurring at the indium/underbump metal interface. Understanding the metallurgical phenomena that drive interfacial evolution over time is key to understanding performance and reliability as a function of processing conditions, shelf-life storage, service conditions, etc. Intermetallics are generally brittle, which can shift failure modes from ductile, cohesive failure to brittle, interfacial failures. Interfacial failures often tend to "unzip" quickly along an entire bond line under low loads. Electrical and/or thermal conduction through these brittle materials may not occur as designed, either.

While the intermetallic compound (IMC) may cause inherent joint performance issues, sometimes it isn't necessarily the intermetallic but rather, the process by which the intermetallic forms: in most cases this is diffusion driven. Diffusion at these interfaces is a bidirectional movement of atoms, but if certain elemental atoms diffuse faster than a counterpart, Kirkendall voids will develop at the interface. A significant number of voids will wreak mechanical and electrical havoc.

Figure 3 shows an SEM image of 2 indium microbumps comprising a thermocompression bond. A small IMC layer at the In-UBM interface, the inherent source of a metallurgical bond, is highlighted by the blue arrow. Since the interface is a non-equilibrium, dynamic environment the

formation, growth, and evolution of this layer is key in the corresponding performance and reliability of this bond.
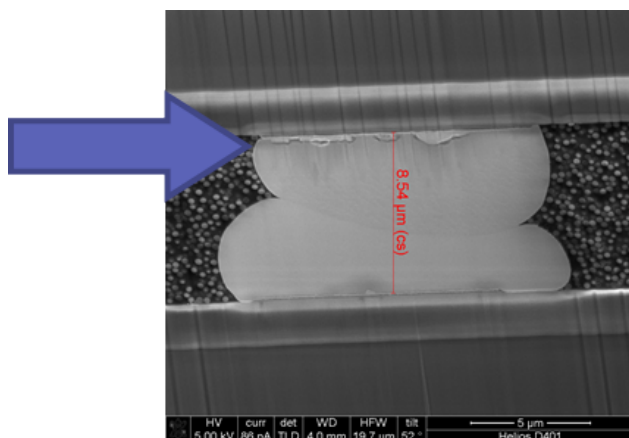

Figure 3. SEM image of an indium microbump, thermocompression bond, courtesy of Matt Jordan.

Indium bump characterization poses a challenge. Traditional mechanical sectioning and polishing is difficult in part because of the small size of the bumps, but also because indium is so soft relative to the other materials adjacent to it. Based on literature and previous work Sandia has developed a cryogenic sectioning technique that utilizes a focused ion beam (FIB) [10,11].

Modeling this interface layer and corresponding reactions is also a challenge. We have been unable to locate interatomic potentials for In-Ni alloys in the literature, and the system of interest (In bumps) are too large to model with density functional theory. However, we can compute some fundamental materials properties that give us insight into the system behavior.

The current evaluation leans on data from previous kinetic evaluations performed at Sandia (pending JEM article). The objective here is to understand how parameters such as underbump metallurgy (UBM) and bump size correspond to mechanical performance while also developing small scale modeling methods to help predict the interfacial reactions

APPROACH

Details regarding fabrication, aging, characterization, testing, and modeling are provided below. Table 1 highlights the variables of interest and the correlating work that has been done or is planned. The cells that are grayed out indicate work that has been previously performed and reported. This previous work guided aging parameters for the more recent work.

Table 1. Summary of the UBM composition and sizes used (or planned for use) in the kinetic and mechanical aging studies.

UBM	Calculated IMC growth parameters			Failure Loads (mN)		Failure Modes	
	Bump Diam. (um)	Act. Energy (kJ)	Time Exponent (n)	As-fab	Aged (125C 100days)	As-fab	Aged (125C, 100days)
TiNi	4						
	6						
	8						
	10	73.2	0.66	0.897	TBD	ductile, In-Ni interface	TBD
	12						
	14						
TiNiAu	10	23.4	0.28	1.115	TBD	ductile, no Au signal	TBD
TiCuNi	10	53	0.34	3.063	TBD	ductile through solder	TBD

Sample Fabrication

To understand underbump metallurgy effects on interface evolution nominal 10 µm diameter, 21 µm pitch indium bumps were fabricated with 3 different underbump metallurgies (UBMs):

1. Ti/Ni (100/100 nm) + 3 µm In
2. Ti/Ni/Au (100/100/20 nm) + 3 µm In
3. Ti/Cu/Ni (50/300/965 nm) + 3 µm In

UBMs 1 and 2 were fabricated using a liftoff process followed by evaporation of indium [12].

UBM 3 was processed differently to achieve a very thick Ni layer; the Ti/Cu film is deposited across the entire wafer to form a seed layer for electroplating. The same negative tone photoresist was used as a mold for Ni electroplating. Indium was then evaporated onto the surface with the photoresist mold intact to perform a similar liftoff. The resulting UBM is wider than the deposited indium bump due to the photoresist profile and the directional evaporation.

When the bump sizes are varied, only UBM 1 is considered, at this point in the evaluation.

Aging

For the kinetic parameter calculations and mechanical testing, the maximum aging condition was 100 days at 125C. At this condition interface reactions were essentially completed, and the characterization indicates a "worst case scenario."

For the variable bump size comparisons, samples were aged for 1 day at 125C in an attempt to observe the interface prior to complete reaction between the UBM and the indium. The goal was to highlight any obvious rate reaction differences as an effect of bump size.

Characterization

Optical imaging, X-ray diffraction (XRD), scanning electron microscopy/energy dispersive spectroscopy (SEM/EDS), and transmission electron microscopy (TEM) were used to image and characterize structure and composition of the interface reaction layers and corresponding layer thicknesses.

Mechanical Testing

Individual In bumps were sheared using an in-house mechanical probe instrument. Ten bumps per UBM were tested.

Modeling

Density functional theory (DFT) calculations were done in VASP (v5.4.4) using the standard PAW_PBE pseudopotentials (Ni 02Aug2007 and In 08Apr2002) with an energy cutoff of 375 eV [6x6x6] kpoints and Methfessel-Paxton (order 1) smearing with a sigma value of 0.2 [13-16]. The exchange-correlation density functional was PBE [17]. The self-consistent field convergence criterion was 0.00001 and minimizations were performed with a maximum force criterion of 0.01 eV/Å. Elastic properties were computed using the "IBRION=6" flag to compute the Hessian matrix.

Formation energies were computed using

$$E_{form} = E_{vac} - E_{pristine} + E_{atombulk}$$

Where E_{form} is the defect formation energy, E_{vac} is the energy of the InNi alloy with a vacancy defect, $E_{pristine}$ is the energy of the perfect InNi crystal with no defect, and $E_{atombulk}$ is the energy of a single In or Ni atom in a perfect bulk crystal.

RESULTS

Characterization, mechanical testing, and modeling results are provided below.

Characterization

Figure 4 shows cryoFIB sections of 10 um diameter bumps for the 3 different UBM stackups in the as-received condition (about 10 days at room temperature). Top-down optical images for the variable bump sizes are also shown for UBM 1. Variable bump sizes were *only* fabricated for this UBM stackup. Reaction layers are evident for UBMs 2 and 3 at this magnification.
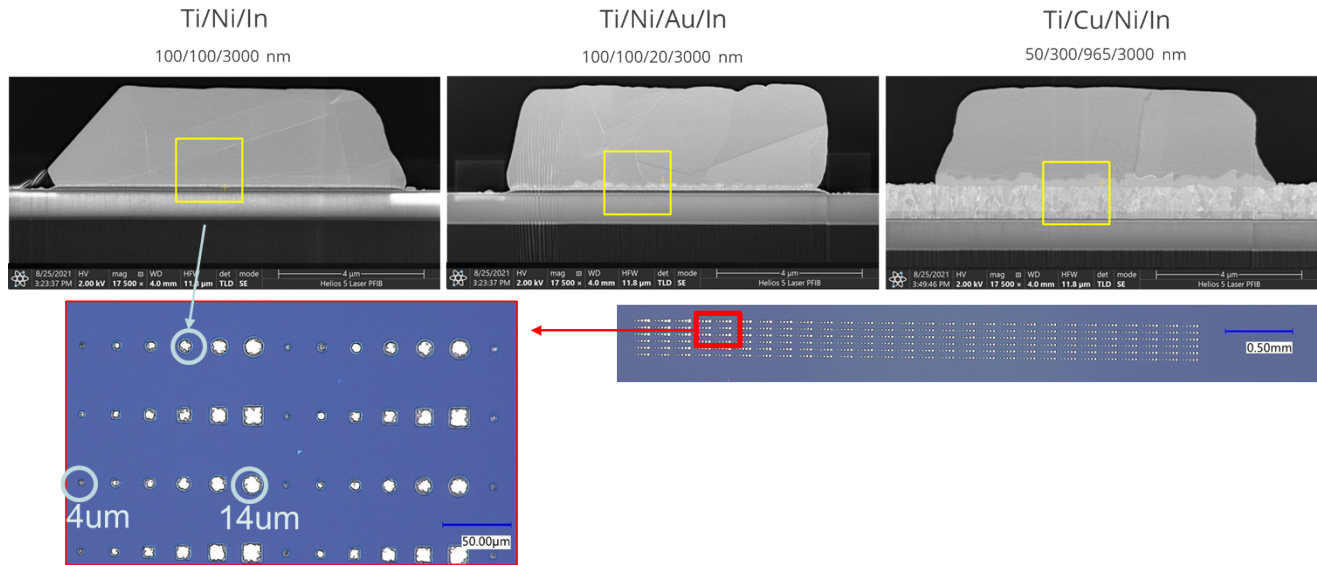

Figure 4. CryoFIB sections of 10 um diameter bumps for the 3 different UBM stackups (UBM 1, 2, 3, left to right, respectively) in the as-received condition (about 10 days at room temperature). Top-down optical images for the variable bump sizes are also shown for UBM 1.

Figure 5 highlights the UBM 1 XRD data for as-received bumps and aged bumps. The highly oriented TI, Ni, and In are all observed, as expected. A peak indicating Ni_3In_7 is also observed, suggesting that the Ni layer is consumed in a reaction with In to form this IMC structure.
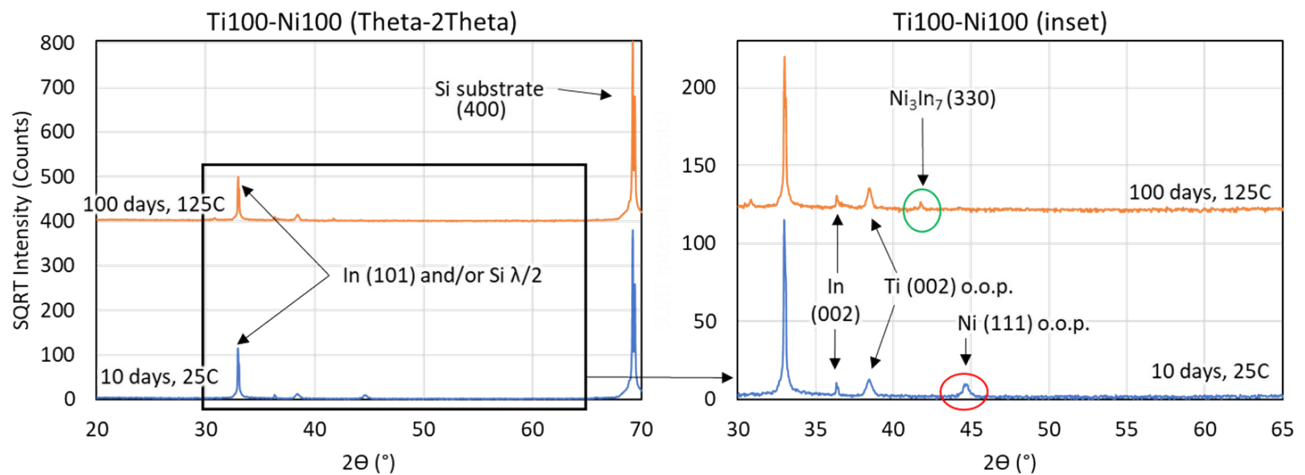

Figure 5. XRD data for as-received bumps (blue) and highly aged (orange) bumps on the UBM1 (Ti/Ni) stackup. The red circle highlights a peak that reduces with aging, and the green circle highlights a peak that forms with aging.

TEM also suggests Ti_2In_5 also develops, as shown in Figure 6.
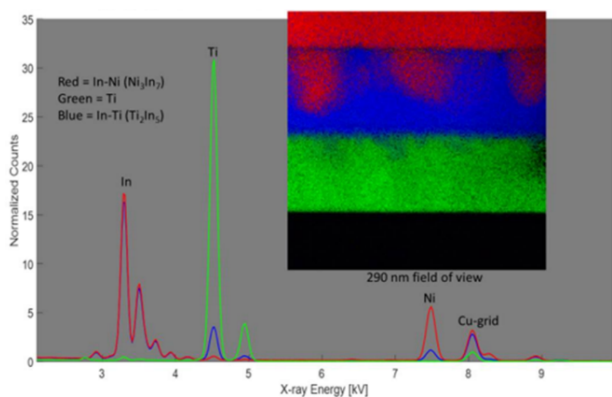
Figure 6. TEM composition map and corresponding count data which suggests a Ti-In reaction is occurring in addition to Ni-In.

Figure 7 shows XRD data for UBM1 after only 1 day at 125C, rather than 100 days. Only elemental Ti, Ni, and In were observed. No intermetallic signals were measured.
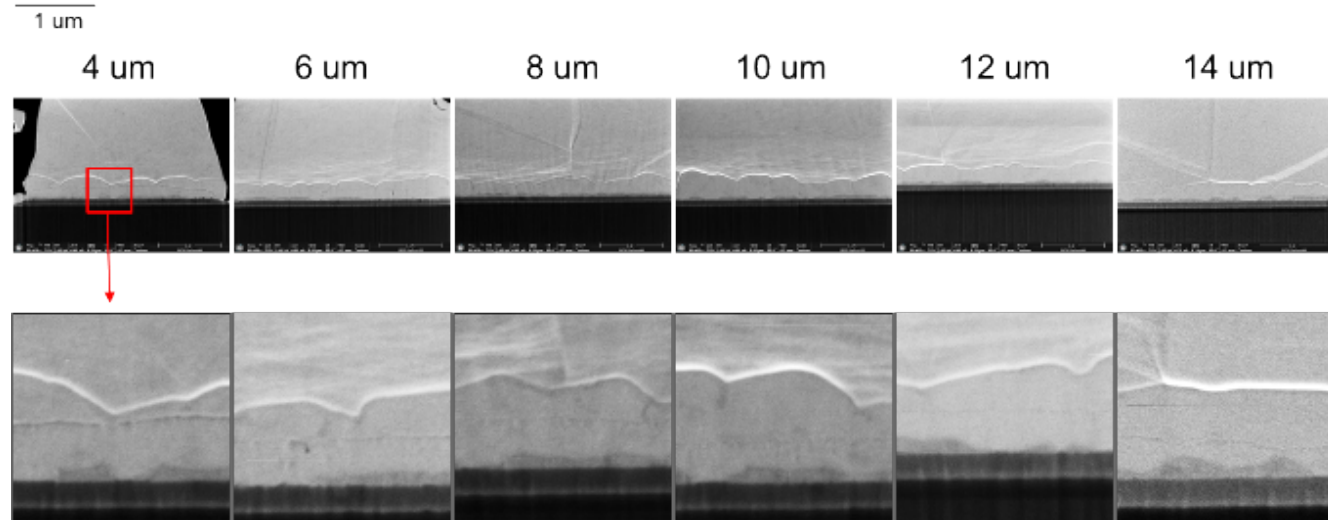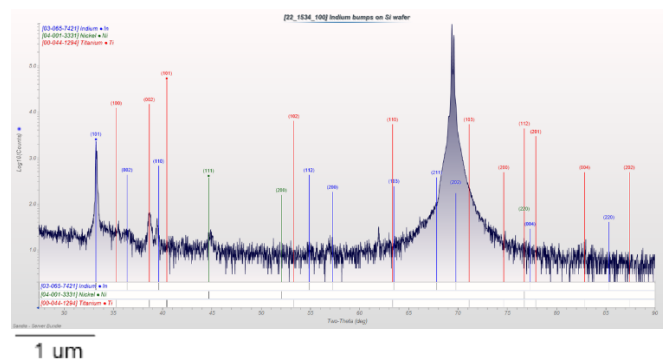

Figure 7. XRD data for UBM 1 after only 1 day at 125C.

The bumps were sufficiently small that any IMC should not have been shielded. Figure 8 shows a low magnification cryoFIB/SEM section through the UBM1 bumps sized 4-14 um, and Figure 9 shows higher magnification SEM images of the respective interfaces. Corresponding EDS maps highlight In, Ni, and Ti signals over the area of 4 different sized bumps in Figure 10.
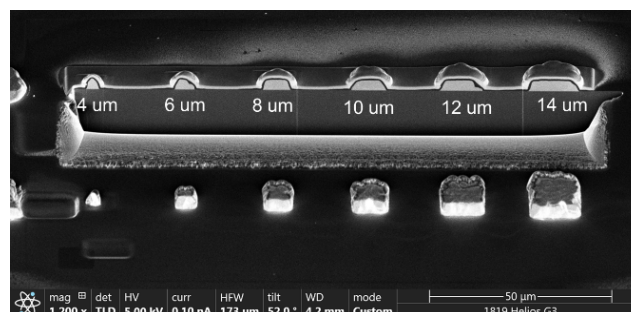

Figure 8. Low magnification cryoFIB/SEM section through the UBM1 bumps sized 4-14 um, left to right, respectively.

Figure 9. High magnification SEM images of the interfaces for the UBM1 bumps sized 4-14 um, left to right, respectively.

A clear reaction zone in all bump sizes is present. Qualitatively, the total thicknesses appear similar over the current size scale. A horizontal line appears within the reaction zone in all bumps.
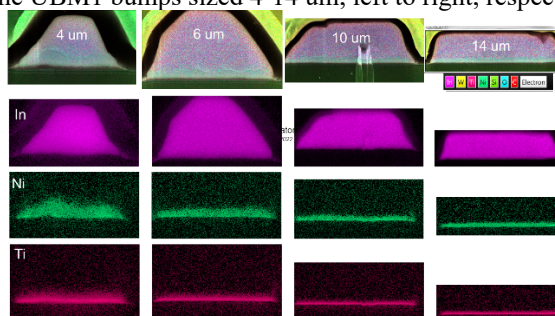
Figure 10. SEM/EDS maps highlighting In, Ni, and Ti signals over the area of 4 different sized bumps, small to large from left to right, respectively.

Ni and Ti diffusion into the In bumps is evident.

Figures 11-13 highlight shear testing data from the as-received bumps (10 um diameter) for all 3 UBMs. Figure 11 shows top-down optical images for each UBM and corresponding load-displacement data.
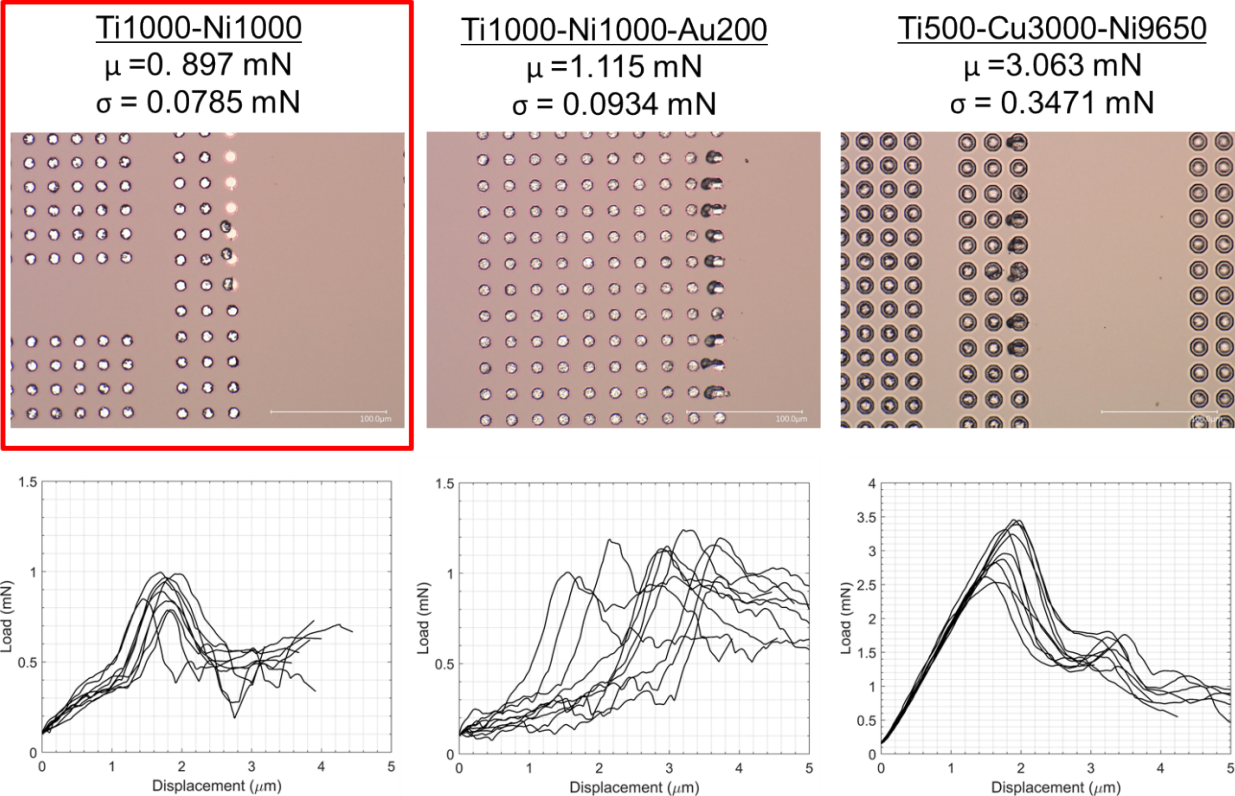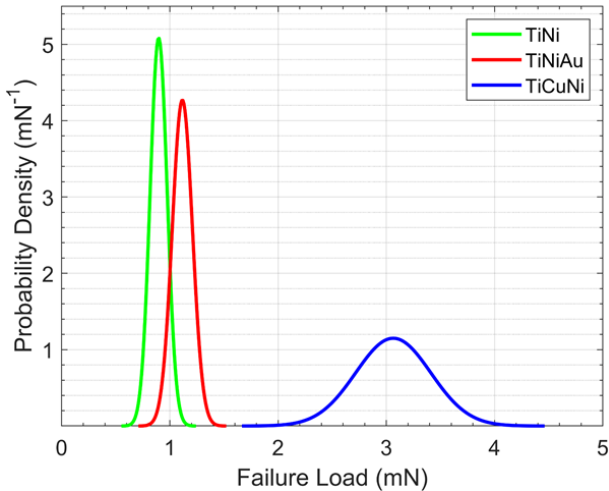
Shear Testing

Figure 11. Post-shear test top-down optical images for TiNi, TINiAu, and TiCuNi as-received UBMs (left to right, top row) and corresponding load-displacement data (left to right, bottom row).

Figure 12. Distributions of the peak loads for 10 bumps per UBM.

The TiCuNi UBM produces the highest peak failure load. The TiNi UBM produces the lowest peak failure load. Distributions of the peak loads for 10 bumps per UBM are shown in Figure 12.

The 3 distinct failure populations confirm the significance of the failure data. Fracture surfaces and corresponding SEM/EDS maps for the sheared bumps are shown in Figure 13.
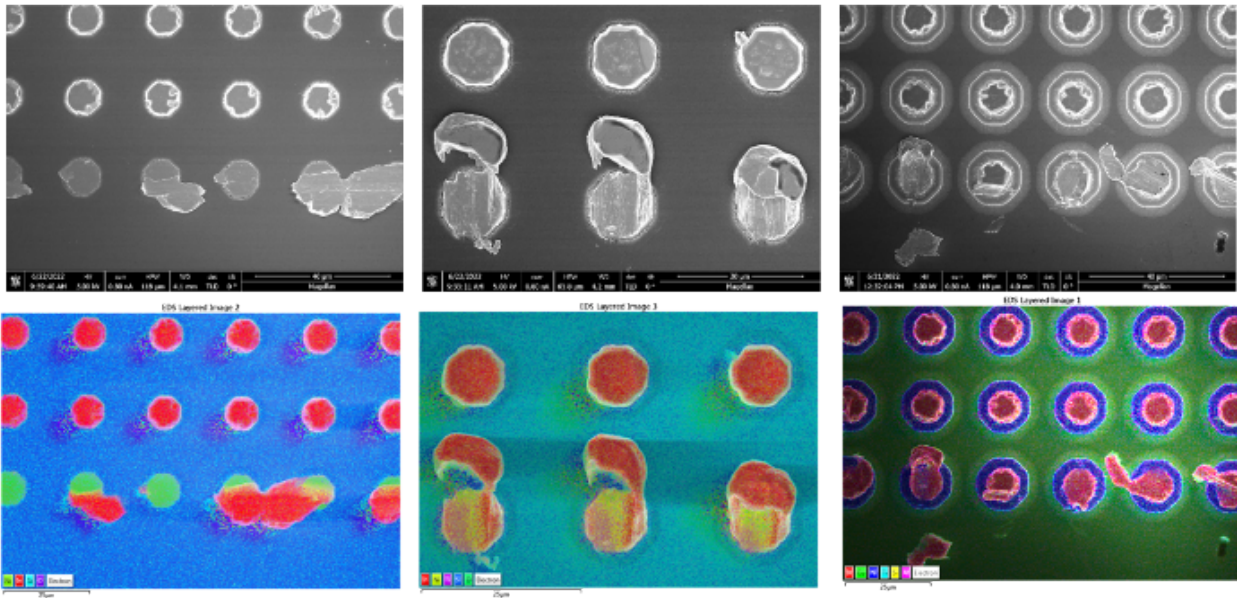
Figure 13. Fracture surfaces (tope row) and corresponding SEM/EDS maps (bottom row)for the sheared bumps corresponding to all 3 UBMS, TiNi, TiNiAu, and TiCuNi, from left to right, respectively.

Clear interfacial failure is observed from UBM 1 (TiNi) along with some ductile failure through the bump. Mostly ductile failure is exhibited by UBM 2 (TiNiAu), and exclusive ductile failure is observed by UBM 3 (TiCuNi).

Complimentary aged data is currently being analyzed.

Modeling
Bulk moduli for In, Ni, and $InNi_2$ and $InNi_3$ intermetallics were computed from DFT. Results are shown in Table 2.

Table 2. Computed bulk moduli values for various In-Ni intermetallic combinations.

Alloy	Bulk Mod (GPa)
In	37.7
$InNi_2$	138.6
$InNi_3$	147.2
Ni	201.0

We also computed vacancy defect formation energies for In, Ni, and various IMCs. Notably, the vacancy formation energy for In was computed to be 0.31 eV, 1.38 eV for Ni, and 0.8 eV for a Ni vacancy in $InNi_3$, and 0.63 eV for a Ni defect in In_3Ni_2.

DISCUSSION

Characterization
CryoFIB is an excellent tool for sectioning small scale In bumps…should greatly enhance current metallurgical understanding of these bump bonds and corresponding interfaces

Metallurgical bonding is confirmed in UBMs 2 and 3 due to the visible reaction layer. UBM 1 may also support metallurgical bonding, but at a much smaller scale. The presence of metallurgical reactions upon fabrication ensures mechanical and electrical contact, but the interface activity over time will impact the reliability and performance of the interconnects during service and/or storage. Significant growth may reduce performance. The 200 nm Au layer added to the Ti/Ni stackup is clearly impacting the interface reactions almost immediately. This may improve manufacturability if the initial TiNi contact isn't ideal, but the impact on lifetime is unknown.

XRD was able to detect intermetallic compounds, though perhaps not all which were present. XRD appears to be a tool which can be exploited to understand interface evolution and layer depletion vs IMC formation. Additional tools such as TEM may still be required. That Ti_2In_5 is a potential IMC suggests that Ti may not be effective in some applications as a diffusion barrier. Whether the entire Ti layer would be completely consumed may require further investigation depending on applications.

Possible that early aging is resulting in elemental diffusion across the interface into a solid solution and intermetallic formation later. This could impact manufacturing and processing condition requirements. Could have noticeable effects on mechanical integrity/electrical properties; needs to be confirmed still

That XRD does not detect Ni_3In_7 after only 1 day at 125C suggests that early on in aging, diffusion across the interfaces is resulting in a solid solution rather than an ordered IMC. The presence of a solid solution may have an extreme impact on mechanical and electrical performance relative to the presence of an ordered, brittle IMC. Fabrication and processing parameters may be used to tune the interface for the desired reaction. Further investigation is currently ongoing to confirm this hypothesis.

Similar thicknesses of the reacted regions from Figure _ indicate that variable bump size isn't significantly impacting reaction rates. However, the fraction of bump that reacts in a smaller bump is much greater than the fraction of bump that reacts in a larger bump suggesting much different performance between the different sizes. Applying the same aging conditions to even larger bumps (i.e. 100 um) may provide even more clarity across size scales.

The apparent horizontal line within the reaction zones of the variable sized bumps has not been further investigated but may indicate the original location of the Ni layer. The SEM/EDS maps confirm qualitative diffusion of both Ni and Ti.

Shear Testing
Fabrication method is impacting mechanical strength. The as-received TiCuNi UBM produces a stronger bond. Ductile failure occurs through the bulk In in all cases, as is desired. The interface is not the weak point. Significant aging is expected to change the bond interfaces significantly though, so significant strength reduction is likely.

The addition of Au also appears to slightly increase the as-received mechanical strength of the bond by shifting the failure location from the Ni-In interface largely into the solder. It is possible that the very small or nearly non-existent IMC in the TiNi stackup is not providing a consistent bond and presents as the weakest link. The addition of Au may jumpstart that interface reaction and provide enough IMC to produce measurable strength but not enough for the brittle properties to reduce the strength. Again, considerable aging is expected to induce significant interface evolution, so mechanical performance is predicted to change significantly. The extent of interface evolution may guide future fabrication parameters.

The current bump shearing method is a good way to assess individual bumps; we are able to measure 3 distinct and significant failure populations but we are approaching size limits; Moving this operation into an SEM would increase resolution and accuracy for bumps smaller than 10um as well as testing consistency; mechanical testing area array bumps is also possible and may be a good way to validate mechanical models.

Additional shear testing of the samples aged for only 1 day at 125C will provide insight into: 1) whether a solid solution reaction is present vs. an intermetallic; and 2) whether there is a significant impact on the mechanical performance of the bond.

Modeling
The elastic properties in Table 2 show that the IMCs $InNi_2$ (139 GPa) and $InNi_3$ (147 GPa) are substantially more brittle than pure In (38 GPa), which demonstrates why IMC formation at the In-Ni interface can result in brittle failure.

Also, the formation energy of defects in the IMCs is fairly low, raning from 0.63 to 0.8 eV for Ni vacancies. While the defect formation energy is lower in In (0.31 eV), these values are still lower than pure Ni (1.38 eV) and suggest that IMC formation could increase the likelihood of defect formation could increase in these IMCs compared to the Ni.

CONCLUSIONS

1. CryoFIB sectioning of In bumps provided excellent surfaces for SEM imaging for bumps in the size range of 4-14 um.
2. Fabrication method has a distinct effect on bond strength. UBM 3 (TiCuNi) produced the highest strength bumps in the as-fabricated condition. More interfacial failures associated with UBM 1 (TiNi) lowered the peak strength relative to UBM 2 (TiNiAu) and suggest that an effective metallurgical bond may not be forming upon fabrication. The added Au in UBM 2 supports the formation of an IMC stronger than just the product of TiNi bonding, but not brittle enough to induce interfacial failure.
3. Initial diffusion between the TiNi layers may be supporting a solid solution composition rather than an ordered IMC. Continued aging appears to promote IMC formation. Strength implications would be expected between a solid solution alloy and an ordered IMC.
4. We expect the aged bumps to behave much differently than the as-received bumps. This upcoming data will be reported.
5. DFT calculations predict that the IMCs are more brittle than In and also prone to forming vacancy defects. This suggests that IMC formation could compromise the strength of the In-Ni interface, possibly resulting in failure.
6. Bump size between 4 and 14 um do not appear to impact reaction rate, but the smaller bumps contain a larger fraction of the reaction product than the larger bumps. Strength correlations to fraction of IMC are expected.
7. Understanding the application requirements for these In bump arrays will be key in driving the necessary fabrication methods, potential heat treatments post-fab, next assembly processing, etc. in order to produce a desired interfacial microstructure to support the desired mechanical and electrical performance and reliability over time.

REFERENCES

1. Massa, Samuel, David Shahin, Ishan Wathuthanthri, Annaliese Drechsler, and Rajneeta Basantkumar. "Process Development for Flip Chip Bonding with Different Bump Compositions." In *2019 International Wafer Level Packaging Conference (IWLPC)*, pp. 1-6. IEEE, 2019.

2. DeNigris, N. S., J. A. Chervenak, S. R. Bandler, M. P. Chang, N. P. Costen, M. E. Eckart, J. Y. Ha, C. A. Kilbourne, and S. J. Smith. "Fabrication of flexible superconducting wiring with high current-carrying capacity indium interconnects." *Journal of low temperature physics* 193, no. 5 (2018): 687-694.

3. Das, R. N., J. L. Yoder, Danna Rosenberg, D. K. Kim, D. Yost, Justin Mallek, David Hover, Vladimir Bolkhovsky, A. J. Kerman, and W. D. Oliver. "Cryogenic qubit integration for quantum computing." In *2018 IEEE 68th Electronic Components and Technology Conference (ECTC)*, pp. 504-514. IEEE, 2018.

4. Zhang, Y., Niu, J., Zhang, P. and Tan, Z., 2020, November. Development of a new indium bump fabrication method for large-area HgCdTe detector. In *AOPC 2020: Infrared Device and Infrared Technology* (Vol. 11563, p. 1156308). International Society for Optics and Photonics.

5. Plötner, M., G. Sadowski, S. Rzepka, and G. Blasek. "Aspects of indium solder bumping and indium bump bonding useful for assembling cooled mosaic sensors." Microelectronics International (1991).

6. Cruz-Campa, Jose L., Gregory N. Nielson, Anthony L. Lentine, Anton A. Filatov, Paul J. Resnick, Carlos A. Sanchez, Adam M. Rowen, Murat Okandan, Vipin P. Gupta, and Jeffrey S. Nelson. "Fabrication of lattice mismatched multijunction photovoltaic cells using 3D integration concepts." In *2012 38th IEEE Photovoltaic Specialists Conference*, pp. 000932-000936. IEEE, 2012.

7. Gee, James M. "Voltage-matched configurations for multijunction solar cells." In *Presented at the 19th IEEE Photovoltaic Specialists Conference*. 1987.

8. Lentine, Anthony L., Gregory N. Nielson, Murat Okandan, William C. Sweatt, Jose L. Cruz-Campa, and Vipin Gupta. "Optimal cell connections for improved shading, reliability, and spectral performance of microsystem enabled photovoltaic (MEPV) modules." In *2010 35th IEEE Photovoltaic Specialists Conference*, pp. 003048-003054. IEEE, 2010.

9. Vahanen, S. "Introduction to High-density interconnection technologies on silicon wafers." CERN (2010).

10. de Morais, L. Dantas, Sophie Chevalliez, and Stephanie Mouleres. "Low temperature FIB cross section: Application to indium micro bumps." *Microelectronics Reliability* 54, no. 9-10 (2014): 1802-1805.

11. Michael, J., Perry, D., Cummings, D., Walraven, J., & Jordan, M. (2022). Focused Ion Beam Preparation of Low Melting Point Metals: Lessons Learned From Indium. *Microscopy and Microanalysis, 28*(3), 603-610. doi:10.1017/S1431927622000496

12. Hollowell, A., et al. "Die Level Microbumping and Flip Chip Bonding for MPW Die." GOMAC, Presentation. 2019.

13. G. Kresse and J. Hafner, Phys. Rev. B 47 , 558 (1993); ibid. 49 , 14 251 (1994).

14. G. Kresse and J. Furthmüller, Comput. Mat. Sci. 6 , 15 (1996).

15. G. Kresse and J. Furthmüller, Phys. Rev. B 54 , 11 169 (1996).

16. M. Methfessel and A.T. Paxton, *Ibid*., **40**, No. 6, 3616 (1989).

17. JP Perdew, K Burke, M Ernzerhof, Physical review letters 77 (18), 3865